The Astrophysical Journal Letters, 735:L34 (6pp), 2011 July 10 doi:10.1088/2041-8205/735/2/L34

EVOLUTION OF GALAXY STELLAR MASS FUNCTIONS, MASS DENSITIES, AND MASS-TO-LIGHT RATIOS FROM $z \sim 7$ TO $z \sim 4$

Valentino González[1], Ivo Labbé[2,5], Rychard J. Bouwens[1], Garth Illingworth[1], Marijn Franx[3], and Mariska Kriek[4]
[1] Astronomy Department, University of California, Santa Cruz, CA 95064, USA
[2] Carnegie Observatories, 813 Santa Barbara Street, Pasadena, CA 91101, USA
[3] Leiden Observatory, Leiden University, NL-2300 RA Leiden, The Netherlands
[4] Department of Astrophysical Sciences, Princeton University, Princeton, NJ 08544, USA
Received 2010 August 23; accepted 2011 May 19; published 2011 June 21

ABSTRACT

We derive stellar masses from spectral energy distribution fitting to rest-frame optical and UV fluxes for 401 star-forming galaxies at $z \sim 4$, 5, and 6 from Hubble-WFC3/IR camera observations of the Early Release Science field combined with the deep GOODS-S *Spitzer*/IRAC data (and include a previously published $z \sim 7$ sample). A mass–luminosity relation with strongly luminosity-dependent $\mathcal{M}/L_{\rm UV}$ ratios is found for the largest sample (299 galaxies) at $z \sim 4$. The relation $\mathcal{M} \propto L_{\rm UV,1500}^{1.7(\pm 0.2)}$ has a well-determined intrinsic sample variance of 0.5 dex. This relation is also consistent with the more limited samples at $z \sim 5$–7. This $z \sim 4$ mass–luminosity relation, and the well-established faint UV-luminosity functions at $z \sim 4$–7, are used to derive galaxy mass functions (MFs) to masses $\mathcal{M} \sim 10^8$ at $z \sim 4$–7. A bootstrap approach is used to derive the MFs to account for the large scatter in the $\mathcal{M}$–$L_{\rm UV}$ relation and the luminosity function uncertainties, along with an analytical cross-check. The MFs are also corrected for the effects of incompleteness. The incompleteness-corrected MFs are steeper than previously found, with slopes $\alpha_M \sim -1.4$ to -1.6 at low masses. These slopes are, however, still substantially flatter than the MFs obtained from recent hydrodynamical simulations. We use these MFs to estimate the stellar mass density (SMD) of the universe to a fixed $M_{\rm UV,AB} < -18$ as a function of redshift and find an SMD growth $\propto (1+z)^{-3.4 \pm 0.8}$ from $z \sim 7$ to $z \sim 4$. We also derive the SMD from the completeness-corrected MFs to a mass limit $\mathcal{M} \sim 10^8\ M_\odot$. Such completeness-corrected MFs and the derived SMDs will be particularly important for comparisons as future MFs reach to lower masses.

Key words: galaxies: evolution – galaxies: high-redshift

Online-only material: color figures

1. INTRODUCTION

Measurements of the stellar mass ($\mathcal{M}_{\rm star}$) of high-redshift galaxies ($z \gtrsim 4$) provide important constraints on scenarios of galaxy formation and early evolution. Recent deep near-IR WFC3/IR observations over the Early Release Science (ERS) field (Windhorst et al. 2011) combined with pre-existing deep GOODS IRAC data provide access to the rest-frame UV and optical wavelengths of $4 < z < 7$ star-forming galaxies and hence reasonably accurate estimates of their $\mathcal{M}_{\rm star}/L_{\rm UV}$ ratios and stellar masses. The substantial samples detected with WFC3/IR span a range in $\mathcal{M}_{\rm star}$, allowing, in principle, the derivation of mass functions (MFs).

MFs are fundamental characteristics of the galaxy population but, in practice, they are difficult to compute directly, especially at high redshift because of selection effects, incompleteness, and contamination by interlopers. A simple alternative approach to derive the MF is to start with the well-determined UV luminosity functions (UV-LFs) at these redshifts and convert them to MFs using an average $\mathcal{M}/L_{\rm UV}$ (e.g., McLure et al. 2009). The main advantage is that LFs are corrected for all selection effects in the data and reach very faint limits. It requires, however, the average $\mathcal{M}/L_{\rm UV}$ to be independent of luminosity. The existence at high z of a relatively tight relation between UV luminosity and $\mathcal{M}_{\rm star}$ (Stark et al. 2009) allows us to improve over this approach. We robustly re-derive this relation over a wide range of UV luminosities and combine it with published UV LFs to estimate improved MFs at $4 < z < 7$. Considering the scatter in the $\mathcal{M}_{\rm star}/L_{\rm UV}$ also allows us to correct for incompleteness at low $\mathcal{M}_{\rm star}$.

We adopt a $(H_0,\ \Omega_M,\ \Omega_\Lambda) = (70\,{\rm km\,s^{-1}\,Mpc^{-1}},\ 0.3,\ 0.7)$ cosmology. All magnitudes are in the AB system (Oke & Gunn 1983).[6]

2. GALAXY SAMPLE FROM *HST* AND *SPITZER* DATA

The sources used here for determinations of the $\mathcal{M}/L$ ratios and $z = 4$–6 MFs were found in the recent Hubble-WFC3/IR observations of the ERS field. Both the GOODS Advanced Camera for Surveys optical ($B_{435}V_{606}i_{775}z_{850}$) and the WFC3/IR ($Y_{098}J_{110}H_{160}$) data reach depths of $\sim$28 mag (5σ, $0\farcs35$ diameter apertures; see Bouwens et al. 2010; Giavalisco et al. 2004). All sources have *Spitzer*/IRAC coverage with depths of 27.8 and 27.1 in the [3.6] and [4.5] channels, respectively (1σ in $2\farcs4$ apertures). The $z \sim 7$ sample is taken from (Labbé et al. 2010a).

The $z \sim 4, 5, 6$ sample totals 679 objects, consisting of 524 B, 123 V, and 32 i dropouts that were selected as in Bouwens et al. (2007).

$z \sim 4$ B dropouts:

$$(B_{435} - V_{606} > 1.1) \wedge [B_{435} - V_{606} > (V_{606} - z_{850}) + 1.1] \wedge (V_{606} - z_{850} < 1.6).$$

[5] Hubble Fellow.

[6] All magnitudes/fluxes are in the observed frame except $M_{\rm UV,1500}$ and $L_{\rm UV,1500}$.

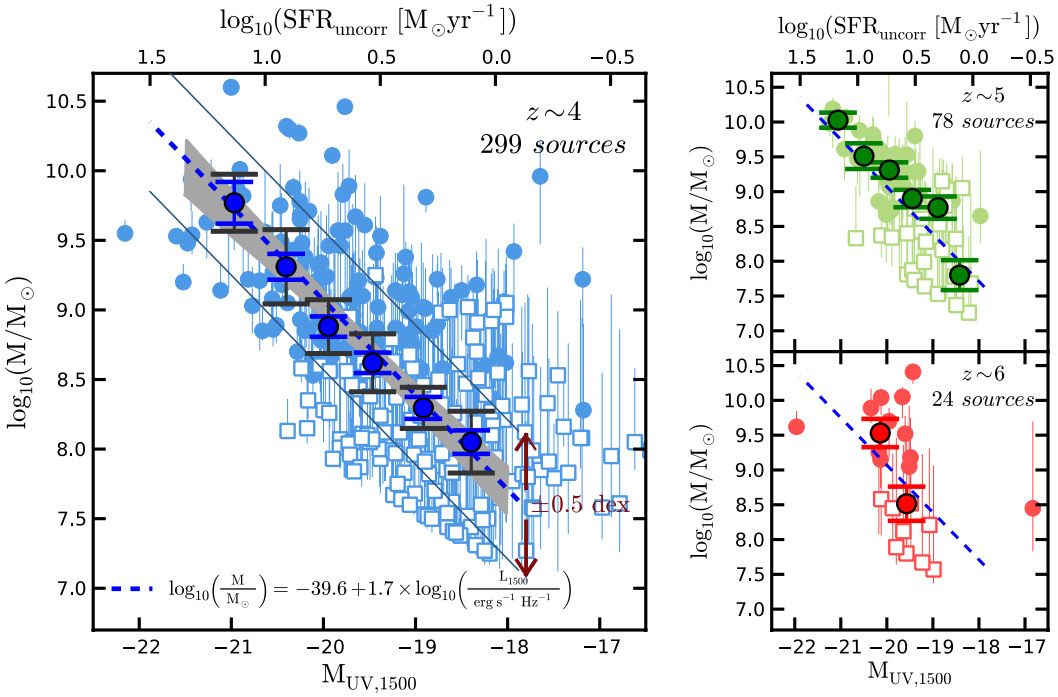

Figure 1. Stellar masses as a function of UV luminosity ($M_{\rm UV,1500} = 51.63 - 2.5 \times \log_{10}(L_{\rm UV,1500}\,[{\rm erg\,s^{-1}\,Hz^{-1}}])$) for the $z \sim 4$, 5, and 6 samples. $\rm SFR_{uncorr}$ (top axis) is derived using the Madau et al. (1998) conversion formula (no extinction correction). The final sample of 401 sources with FAST SED-fit mass estimates is shown here. Open squares indicate low-S/N measurements ($<2\sigma$ in [3.6]). The larger symbols in each panel represent the median mass of the sample ($\sim$0.5 $M_{\rm UV,1500}$ mag bins). The small error bars represent the bootstrapped errors. The larger black error bars include a conservative estimate of the systematics computed by comparing the estimated median mass at a given luminosity with the mass estimated from the stacked SEDs at the same luminosity. The dashed blue line (and shaded area, slope $= 1.7 \pm 0.2$) represents the median $\log_{10}\mathcal{M}$–$\rm M_{UV,1500}$ trend at $z \sim 4$. It is consistent with no evolution with redshift. The scatter at the luminous end ($\pm$0.5 dex), where photometric errors are small, is intrinsic (see Figure 2).

(A color version of this figure is available in the online journal.)

$z \sim 5$ V dropouts:

$$\{[V_{606} - i_{775} > 0.9(i_{775} - z_{850})] \vee (V_{606} - i_{775} > 2)\}$$
$$\wedge\, (V_{606} - i_{775} > 1.2) \wedge (i_{775} - z_{850} < 1.3).$$

$z \sim 6$ i dropouts[7]:

$$(i_{775} - z_{850} > 1.3) \wedge (z_{850} - J_{125} < 0.8).$$

The rest-frame optical photometry from *Spitzer*/IRAC is ideally suited for deriving stellar masses at these redshifts (e.g., Papovich et al. 2001; Yan et al. 2005; Eyles et al. 2005; Labbé et al. 2010a). A challenge is that the broad IRAC point-spread function usually results in these faint sources being contaminated by foreground neighbors. To obtain reliable IRAC fluxes we use the deblending method of Labbé et al. (2006; see also González et al. 2010; Labbé et al. 2010a, 2010b; Wuyts et al. 2007; de Santis et al. 2007). Briefly, this method uses the higher-resolution *Hubble Space Telescope* (*HST*) images to create models of both the foreground neighbors and the source itself. We convolve each model image with a kernel to simulate the IRAC observations. We fit for all the sources simultaneously (with independent normalization factors) and subtract the best fits for the neighbors. In the clean image of each dropout we are able to perform standard aperture photometry. We use 2.″5 diameter apertures and correct the fluxes to total assuming stellar profiles (1.8× in both channels).

As expected, our cleaning procedure does not work for every source. We restrict our sample to the 60% of sources with the best χ^2 residuals. This reduces the number of non-optimal subtractions to <8%. The final sample suitable for deriving masses from the *HST* + *Spitzer* data totals 401 sources: 299 at $z \sim 4$, 78 at $z \sim 5$, and 24 at $z \sim 6$. We do not expect this selection step to introduce any important biases, since it depends on the distribution of the non-associated neighbors of the source. Of the remaining sources, ∼50% have low IRAC signal-to-noise ratio (S/N; $<2\sigma$ in [3.6]).

3. STELLAR MASS ESTIMATES FROM SED FITS

We use the FAST spectral energy distribution (SED) fitting code (Kriek et al. 2009) to derive $\mathcal{M}_{\rm star}$ for the 401 $z \sim 4$–6 sources. We fit their SEDs with the full suite of fitted parameters. For all sources we fit the broadband ACS + WFC3/IR + IRAC [3.6] and [4.5] fluxes using the Bruzual & Charlot (2003, BC03) models with a Salpeter (1955) initial mass function (IMF; 0.1–100 $M_\odot$) and assuming a 0.2 $Z_\odot$ metallicity. We also include the sample of $z \sim 7$ galaxies with similarly determined masses from Labbé et al. (2010a).

The star formation history (SFH) cannot be uniquely determined from broadband SEDs due to well-known degeneracies between the star formation timescale, age, and dust extinction. We have assumed an SFH with a constant star formation rate (SFR). Different SFHs introduce systematic offsets to the mass determinations, largely independent of redshift (cf. Papovich et al. 2011). The systematic differences between masses based on declining, constant, or rising SFHs are typically $\lesssim$0.3 dex (Finlator et al. 2007).

Figure 1 (left) shows the FAST SED-fit $\mathcal{M}_{\rm star}$ (from *HST* + *Spitzer* data) versus UV luminosity (bottom axis).

[7] Slightly modified.

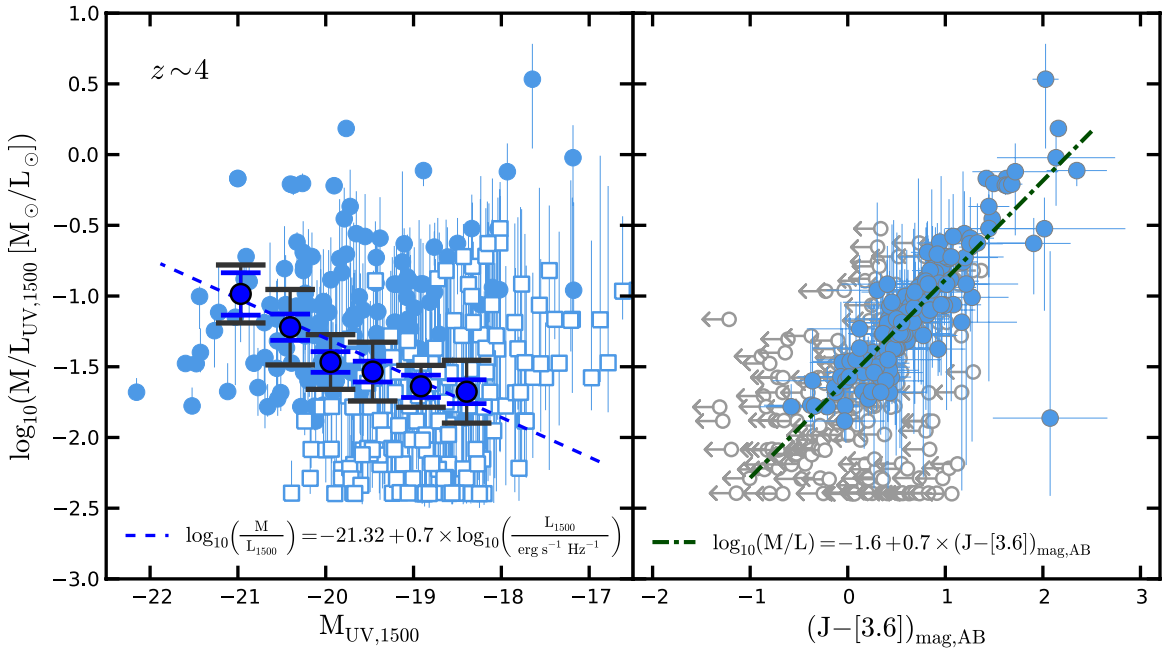

Figure 2. Left: $\mathcal{M}/L$ ratio as a function of UV luminosity for the $z\sim4$ sample. Symbols and error bars are as in Figure 1. The median $\mathcal{M}/L$ ratio changes by a factor 5× in the luminosity range of our sample. Right: the correlation between the $\mathcal{M}/L$ and $J-[3.6]$ color. Arrows indicate 2σ upper limits. This tight relation suggests that the large scatter observed in the $\mathcal{M}/L$ (left panel) is largely due to intrinsic variations in the UV-to-optical colors. Photometric scatter can only account for $\lesssim$0.14 dex at $M_{\mathrm{UV},1500}\sim-20$ (0.37 dex at -19).

(A color version of this figure is available in the online journal.)

While the scatter is large (rms $\sim$ 0.5 dex), there is a clear trend of increasing mass with increasing UV luminosity. The $\mathcal{M}_{\mathrm{star}}$–$L_{\mathrm{UV},1500}$ relation at $z\sim4$ is well fit by $\log_{10}(\mathcal{M})\propto1.7(\pm0.2)\log_{10}(L_{1500})$. The lower bound that appears at $\mathcal{M}_{\mathrm{star}}<10^8\,M_\odot$ corresponds to the $\mathcal{M}/L$ of the youngest model we allow (10 Myr). The existence of this limit is not critical since our inferred $\mathcal{M}/L$ trend slope (and its uncertainty) is insensitive to the cutoff. This is confirmed by a stacking analysis which shows significant IRAC detections in the faintest bins ($>3\sigma$), and good agreement in the slopes (and uncertainties) derived. We remark that the broadband fluxes appear to be dominated by continuum light and not emission lines, as indicated by the similar median-stacked [3.6] and [4.5] IRAC fluxes. The $z\sim4$ relation is consistent with the $z\sim5$ sample, and, in zero point, with the small $z\sim6$ sample and the $z\sim7$ sample presented in Labbé et al. (2010a).

Figure 2 explores the $z\sim4$ $\mathcal{M}/L$ ratio trend in more detail, showing that $\mathcal{M}/L_{\mathrm{UV},1500}$ depends on luminosity; the $\mathcal{M}/L$ ratio is ∼5× lower at $M_{\mathrm{UV},1500}=-18$ than at $M_{\mathrm{UV},1500}=-21$. This suggests that UV-faint galaxies contribute less to the global stellar mass density (SMD) than assumed in previous studies (Labbé et al. 2010a, 2010b). Their contribution may still be significant at $z\gtrsim7$ given the steeper faint-end slopes of the UV-LF (Bouwens et al. 2010).

A striking aspect of the relation is the large scatter in $\mathcal{M}/L$. The observed sample variance (one standard deviation) for our sample is ∼0.5 dex for $-21<M_{\mathrm{UV},1500}<-18$. At the bright end $M_{\mathrm{UV},1500}<-20$ the scatter is largely intrinsic, whereas at the faint end $M_{\mathrm{UV},1500}>-19.5$ it is dominated by observational uncertainties. In particular, the $\mathcal{M}_{\mathrm{star}}$ of sources with IRAC detections are much better constrained than IRAC-undetected sources. We find that the $\mathcal{M}/L$ ratio is tightly correlated with the $J-[3.6]$ color (standard deviation 0.18 dex; Figure 2, right), suggesting that the variation is real, and not an artifact of the modeling. Photometric uncertainties contribute ∼0.14 dex to the scatter at $M_{\mathrm{UV},1500}\sim-20$ (0.37 dex at -19).

The relation in Figure 2 (right) also allows us to estimate the possible effect of contamination by emission lines (not included in our models). At $z\sim4$, a 20% contribution of Hα to [3.6] would result in redder $J-[3.6]$ colors and hence overestimates of the $\mathcal{M}/L$ and of the masses by 30%. This would affect the SMDs at all redshifts because they all rely on our $z\sim4$ $\mathcal{M}/L$ ratio estimates (see Section 4).

4. STELLAR MASS FUNCTIONS AT $z\sim4$, 5, 6, AND 7

Since UV-LFs have been derived from large samples to very faint limits and carefully corrected for a wide range of potential biases, they constitute an excellent basis for determining MFs. However, a meaningful transformation from UV luminosity into stellar mass is not expected in general. Nevertheless, the calibration of log ($\mathcal{M}_{\mathrm{star}}$) versus $M_{\mathrm{UV},1500}$ in Figures 1 and 2 demonstrates that, for star-forming galaxies at $z\sim$ 4–7, such meaningful transformation does exist.

However, the scatter about the mean $\mathcal{M}$–$M_{\mathrm{UV},1500}$ relation is so large that ignoring it would produce significant errors. Galaxies with relatively low luminosity but high $\mathcal{M}/L$ ratios, for example, contribute significantly at the high-mass end of the MFs.[8] Hence, we take care to determine the average $\mathcal{M}$–$M_{\mathrm{UV},1500}$ relation in a robust way, we characterize its scatter at high masses and use this estimate of the scatter at lower masses/luminosities where the observational uncertainties dominate.

We use two approaches to create the MFs. First, we use the individual best-fit values in Figure 1 (small circles and squares) as representative of the $\mathcal{M}$–$M_{\mathrm{UV},1500}$ distribution by bootstrap re-sampling them. We sample the best-fit values only

[8] Massive UV-faint, passively evolving red galaxies may be missing from our sample. Given the young age of the universe, their numbers are expected to be low.

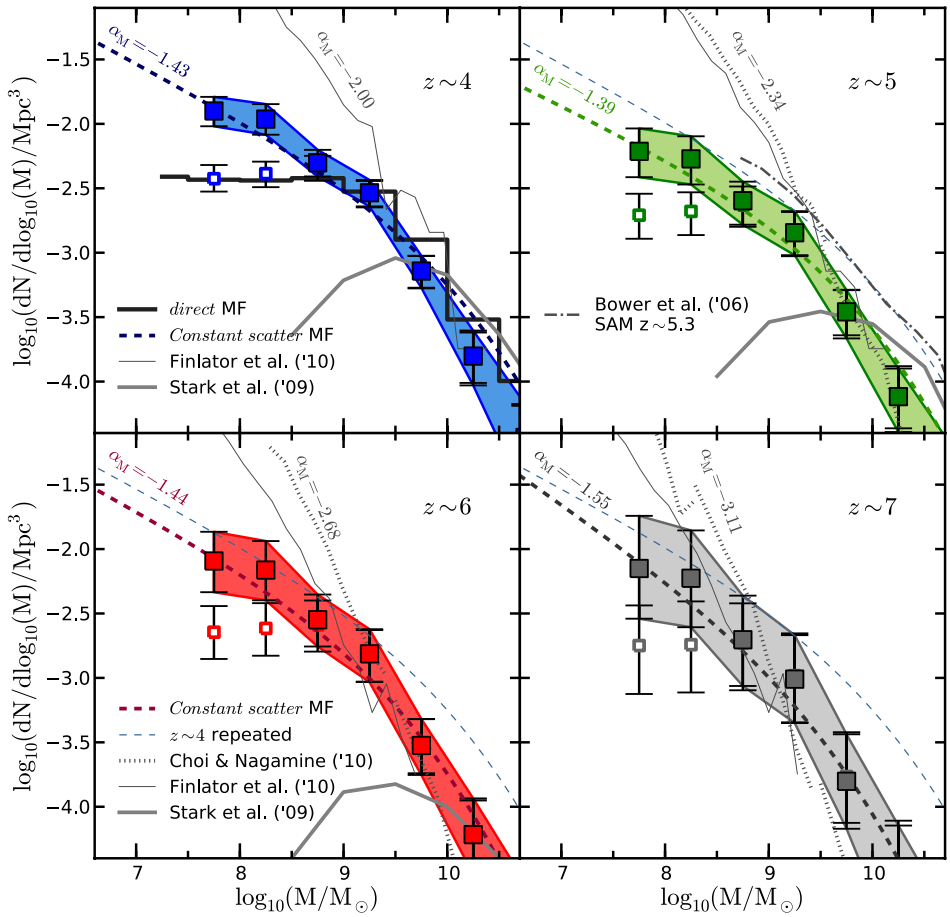

Figure 3. Stellar mass functions at $z\sim4$, 5, 6, and 7 derived from the $\log(\mathcal{M})$–$M_{\rm UV,1500}$ distribution for the $z\sim4B$ dropouts (Figure 1), and the Bouwens et al. (2007, 2010) UV-LFs at $z\sim4$–7. The points are derived from the "bootstrap" approach (see the text). Errors reflect uncertainties in the LF and the ∼0.5 dex 1σ scatter of the $\mathcal{M}$–$M_{\rm UV,1500}$ relation (Figure 1). Completeness-corrected values are estimated assuming that the $\mathcal{M}$–$M_{\rm UV,1500}$ relation extends to fainter limits with similar scatter about the extrapolated mean trend ($M_{\rm UV,1500}<-18$ uncorrected: open; corrected: filled; dark band is at 1σ around the corrected values). The direct MF at $z\sim4$ (thick histogram) is in good agreement with the uncorrected MF (see the text). For masses $>10^{9.5}\,M_\odot$, the uncorrected $z<7$ MFs are in rough agreement with the determinations of Stark et al. (2009) and of McLure et al. (2009) at $z\sim6$ and $\mathcal{M}>10^{10}\,M_\odot$. The thick dashed curve in each panel represents the constant scatter MFs derived from an idealized $\mathcal{M}$–$M_{\rm UV,1500}$ relation (see Section 4). These MFs have low-mass slopes $\alpha_M\sim-1.4$–1.6, slightly flatter than the UV-LFs ($\alpha=-1.7$–2.0: Bouwens et al. 2010). In turn, the assumed symmetric scatter of 0.5 dex flattens their slopes at the high-mass end. The $z\sim4$ constant scatter MF is repeated in the other panels for comparison (thin dashed curve). The dotted and thin solid lines show the simulated MFs from Choi & Nagamine (2010) and Finlator et al. (2011). Our new results are corrected for incompleteness, yet the difference between our results and the simulations is already substantial by $\mathcal{M}=10^9\,M_\odot$. The source of the disagreement is unclear. Tentatively flatter MFs are seen in some SAMs (e.g., Bower et al. 2006 at $z\sim5.3$).

(A color version of this figure is available in the online journal.)

because the scatter dominates the uncertainties. To correct for incompleteness we add faint sources to the distribution. This important step increases the low-mass slope of the MFs substantially. Second, we use the best-fit $\mathcal{M}$–$M_{\rm UV,1500}$ relation (Figure 1, blue dashed line) and an idealized model of its scatter to produce what we label as "constant scatter" versions of the MFs. We compare against other estimates as a cross-check.

Bootstrapped MFs. We start with the $z\sim4$–7, UV-LFs of Bouwens et al. (2007, 2010) and draw 40,000 luminosities from each LF in the range $-21.5<M_{\rm UV,1500}<-18$. We convert the UV luminosities into $\mathcal{M}_{\rm star}$ by assigning $\mathcal{M}_{\rm star}/L_{\rm UV}$ ratios from the distribution of points at $z\sim4$ (Figure 2) with similar UV luminosity. We use the $z\sim4\log(\mathcal{M}/L)-M_{\rm UV,1500}$ distribution at all redshifts because it is well defined over a wide range of luminosities and is consistent with the relations at other redshifts (including the $z\sim7$ relation in Labbé et al. 2010a). To account for the uncertainties in the LFs we perturb their Schechter parameterizations within the uncertainties and repeat 5000 times. This "bootstrap" process results in the uncorrected MFs (Figure 3, open squares and error bars).

As a cross-check we also derived a histogram MF at $z\sim4$ directly from the masses of the $z\sim4$ sample using the search volume for the B dropouts. This straightforward process gives an MF that is identified in Figure 3 as the "direct MF" for comparison with the uncorrected "bootstrap MF."

To correct the MFs for incompleteness at $\mathcal{M}_{\rm star}<10^{8.5}\,M_\odot$, we assume that the observed $\log(\mathcal{M})$–$M_{\rm UV,1500}$ relation extends to UV luminosities below the observed and that the low-luminosity scatter is similar to the scatter around $M_{\rm UV,1500}\sim-18.5$. We use this assumption to populate the $-18<M_{\rm UV,1500}<-15$ range of the $\log(\mathcal{M})$–$M_{\rm UV,1500}$ relation. We re-derive the MFs with these fake sources added. The resulting errors on the corrected points include an added uncertainty that is typically about 30%–40%. This accounts for the LF uncertainties (specially the faint-end slope) and the large scatter about the relations. Other sources of uncertainty may remain but further assessment is needed to fully evaluate them. Regardless, the current corrections must make these corrected MFs a better estimate of the true MFs. Applying the completeness corrections is a crucial step and significantly changes the slope of the MF

Table 1
Summary of Results

Quantity	$\langle z\rangle = 3.8$	$\langle z\rangle = 5.0$	$\langle z\rangle = 5.9$	$\langle z\rangle = 6.8$	$\langle z\rangle = 8.0$
Completeness-corrected Mass Functions					
$\log_{10}(\mathcal{M}/M_\odot)$	$\log_{10}(dN/d\log_{10}(\mathcal{M}/M_\odot)/\mathrm{Mpc}^3)$				
[7.5–8.0]	$-1.90(^{+0.11}_{-0.12})$	$-2.21(^{+0.18}_{-0.20})$	$-2.09(^{+0.23}_{-0.24})$	$-2.15(^{+0.41}_{-0.39})$	...
[8.0–8.5]	$-1.96(^{+0.12}_{-0.12})$	$-2.27(^{+0.18}_{-0.20})$	$-2.16(^{+0.23}_{-0.23})$	$-2.23(^{+0.37}_{-0.38})$	...
[8.5–9.0]	$-2.30(^{+0.10}_{-0.11})$	$-2.60(^{+0.15}_{-0.19})$	$-2.55(^{+0.20}_{-0.21})$	$-2.70(^{+0.34}_{-0.36})$	...
[9.0–9.5]	$-2.53(^{+0.10}_{-0.11})$	$-2.84(^{+0.17}_{-0.17})$	$-2.81(^{+0.19}_{-0.22})$	$-3.01(^{+0.34}_{-0.34})$	...
[9.5–10.0]	$-3.14(^{+0.12}_{-0.13})$	$-3.46(^{+0.17}_{-0.21})$	$-3.52(^{+0.21}_{-0.23})$	$-3.80(^{+0.36}_{-0.37})$	...
[10.0–10.5]	$-3.80(^{+0.20}_{-0.23})$	$-4.12(^{+0.22}_{-0.27})$	$-4.22(^{+0.28}_{-0.31})$	$-4.53(^{+0.39}_{-0.61})$	...
[10.5–11.0]	$-4.43(^{+0.26}_{-0.46})$	$-4.81(^{+0.33}_{-0.45})$	$-4.97(^{+0.38}_{-0.70})$	...	...
SMD ($\mathcal{M} > 10^8\ M_\odot$) [$10^6\ M_\odot$]	$19.27(^{+2.88}_{-2.62})$	$9.64(^{+1.88}_{-1.78})$	$9.76(^{+2.30}_{-1.91})$	$6.98(^{+2.57}_{-2.26})$	...
SMD ($M_{1500} < -18$) [$10^6\ M_\odot$]	$18.96(^{+1.94}_{-1.90})$	$9.52(^{+1.27}_{-1.58})$	$8.79(^{+2.11}_{-1.91})$	$4.08(^{+1.59}_{-1.19})$	$1.8(^{+0.7}_{-1.0})$
Best fit	$\log_{10}(\mathrm{SMD}(z)/[M_\odot\ \mathrm{Mpc}^{-3}]) = 7.00(^{+0.04}_{-0.05}) - 3.35(^{+0.82}_{-0.94}) \times \log_{10}(\frac{1+z}{6})$				

at lower mass. The corrected MFs are shown in Figure 3 by the solid points and the solid color band, and are referred to as the bootstrap MFs.

Constant Scatter MFs. Now we combine the same LFs as above with an idealized version of the $\mathcal{M}$–$M_{\mathrm{UV},1500}$ relation based on the best fit: $\mathcal{M} \propto L_{\mathrm{UV},1500}^{1.7(\pm0.2)}$. Since the scatter is important to reproduce the shape of the MF at the massive end, we generate a slightly more realistic approximation by assuming an idealized log–normal distribution with a constant standard deviation of 0.5 dex around the best-fit relation. The resulting relation, normalized by the LF, is integrated over L to get the constant scatter MFs.

At low masses, the MF slope, α_M, is set by the faint-end slope of the UV-LF, α_L, and the slope, b, of the log ($\mathcal{M}$)–log ($L_{\mathrm{UV},1500}$) relation

$$\alpha_M = \frac{\alpha_L - b + 1}{b},$$

found by extrapolating the $\mathcal{M}$–$L_{\mathrm{UV},1500}$ relation to lower luminosities. We find MFs with steep low-mass slopes of $-1.43(\pm0.11)$, $-1.39(\pm0.11)$, $-1.44(\pm0.15)$, and -1.55 (±0.21) at $z \sim 4, 5, 6$, and 7. These MF slopes are slightly flatter than the UV-LF slopes ($\alpha = -1.7$–2: Bouwens et al. 2010). They are in good agreement with our completeness-corrected bootstrap MFs, and so provide a useful "sanity check" on those results. The standard deviation of 0.5 dex in the log($\mathcal{M}$)–$M_{\mathrm{UV},1500}$ relation results in a slightly enhanced number density at the high-mass end compared to a case with no scatter. Our corrected MFs are considerably steeper than other MF determinations at high redshift (Stark et al. 2009) that do not apply completeness corrections. Truncating the constant scatter $\mathcal{M}$–$M_{\mathrm{UV},1500}$ relation at $M_{1500} < -18$ (to represent survey incompleteness) results in MFs that are in good agreement with the non-corrected bootstrap MFs at low masses.

Comparisons to simulated MFs. The MFs derived here are substantially steeper at low masses than what has been found in the past at these redshifts. This is not unexpected given that it has not been typical to correct for incompleteness. While the corrections are uncertain in magnitude the sign of the correction is not. Interestingly, even with the corrected and steeper slopes, the observed MFs are quite different from what is seen in recent hydrodynamical simulations (e.g., Choi & Nagamine 2010; Jaacks et al. 2011; Finlator et al. 2011). The simulated MFs are steeper, with many more low-mass sources than we find. Tentatively, flatter MFs are seen in semi-analytic models (SAMs; e.g., Bower et al. 2006).

5. STELLAR MASS DENSITY AT $z \sim 4, 5, 6$, AND 7

The MFs can be integrated to determine the SMD of the universe at high redshift. First, we integrate the (uncorrected) bootstrap MFs to determine the SMD at $z = 4, 5, 6$, and 7 to faint-luminosity limits ($M_{1500} < -18$; Table 1; Figure 4, left). Fitting the SEDs using the observed fluxes rather than upper limits allows us to reach lower limits than those of Stark et al. (2009) at $z = 4$–6. To compare to those results, we correct their original $M_{1500} = -20$ limit to our $M_{1500} = -18$ limit by adding 0.18, 0.22, and 0.32 dex at $z \sim 4$, 5, and 6 respectively. We derive an SMD growth across cosmic time that is well fit by the function $\log_{10}(\mathrm{SMD}) \propto (1+z)^{-3.4\pm0.8}$. The effect of a different IMF and of a potential contamination by 20% Hα at $z \sim 5$–6 is also shown in Figure 4.

A major result of this Letter is the derivation of MFs corrected for incompleteness at low masses. To utilize the (more representative and accurate) corrected MFs in deriving the SMD of the universe at high redshift we need to integrate to a fixed mass limit. We choose $\mathcal{M} > 10^8\ M_\odot$ to extend to the limit of our corrected data. The right panel of Figure 4 shows these results, and compares them with the estimates to a fixed luminosity limit (see also Table 1).

The differences are relatively small due to the fact that the SMD is dominated by bright/massive sources already included in the flux-limited ($M_{\mathrm{AB}} < -18$) samples. This depends somewhat on the exact slope of the $\mathcal{M}$–L_{UV} relation but is consistent with the results from the MFs of, e.g., Marchesini et al. (2009) at $3 < z < 4$. Nonetheless, the corrections become more important at higher redshift where the same $M_{\mathrm{AB}} < -18$ limit is applied to a galaxy population with fainter an L^* and steeper LFs. These corrections will become increasingly important as we push our MF estimates to lower masses and higher redshifts.

6. KEY RESULTS

We derive stellar masses from SED fits to *HST* + *Spitzer* data for over 400 $z \sim 4$–7 galaxies. We determine the $\mathcal{M}$–L_{UV}

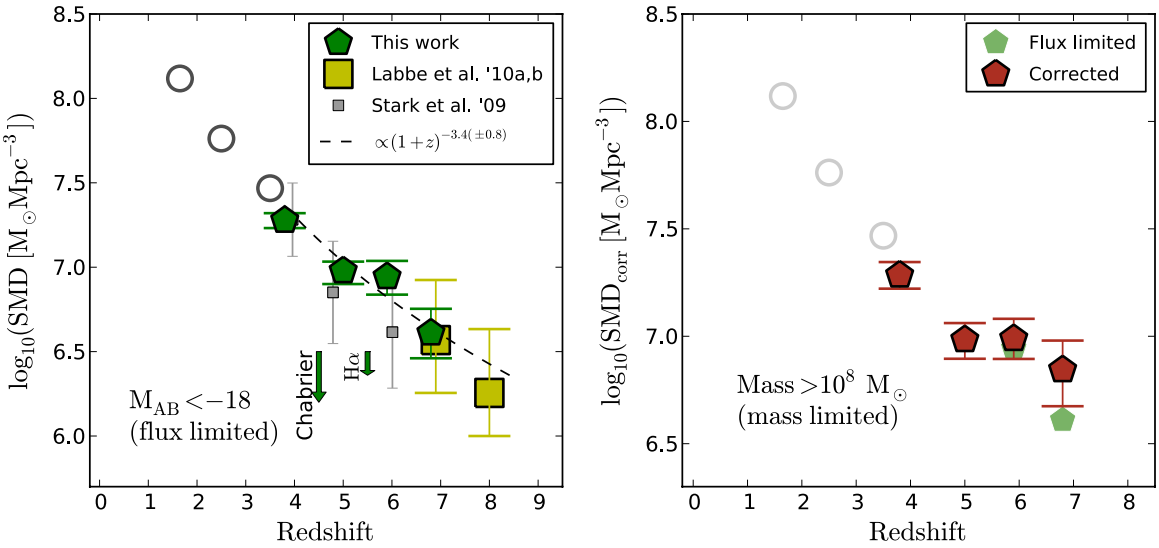

Figure 4. Left: SMD vs. redshift for sources brighter than $M_{\mathrm{UV,1500,AB}} = -18$. These SMD values are derived by integrating the uncorrected bootstrap MFs in Figure 3 to the faint luminosity limit $M_{\mathrm{UV,1500}} = -18$ at $z = 4$, 5, 6, and 7. For comparison, we show the SMD determinations from Stark et al. (2009) corrected from their original $M_{\mathrm{UV,1500}} = -20$ limit to our $M_{\mathrm{UV,1500}} = -18$ limit (see the text). The $z \sim 6$ estimate is also in good agreement with Yan et al. (2006) and Eyles et al. (2007). The low-redshift open circles were derived by integrating the Marchesini et al. (2009) MFs between $8.3 < \log_{10}(\mathcal{M}/M_\odot) < 13$ and multiplying by 1.6 to match the Salpeter IMF. A constant SFH and 0.2 $Z_\odot$ metallicity was assumed to derive the masses at $z \gtrsim 4$. The effect of a possible 20% correction due to contamination by Hα is shown, as is the effect of using a different IMF. Our derived SMD growth with cosmic time is well fit by $\log_{10}(\mathrm{SMD}) \propto (1+z)^{-3.4\pm0.8}$. Right: as for the left panel but now to a fixed $\mathcal{M}_{\mathrm{star}}$ limit $> 10^8 M_\odot$. The mass-limited SMD is compared to the flux-limited values from the left panel. The differences are relatively small (see the text). Nonetheless, the importance of utilizing the completeness-corrected MFs will increase as improved, deeper data become available and we can push to lower masses and higher redshifts.

(A color version of this figure is available in the online journal.)

relation and find it to be steep ($\log(\mathcal{M}) \propto 1.7(\pm0.2)\log(L_{\mathrm{UV}})$) with large intrinsic scatter; the sample variance is ∼0.5 dex at the bright end. We derive MFs by combining the $\mathcal{M}/L$ results with published deep UV-LFs at $z \sim 4$–7, and correct them for incompleteness. The corrected MFs are steeper ($\alpha \sim -1.4$ to -1.6) than found previously, but still far less steep than those from recent hydrodynamical simulations. The integrated SMD of the universe is derived at $z \sim 4$, 5, 6, and 7 to $\mathcal{M} \sim 10^8\ M_\odot$.

We acknowledge insightful discussions with Kristian Finlator, Casey Papovich, Daniel Schaerer, and Daniel Stark. We thank Ken Nagamine, Junhwnan Choi, and Kristian Finlator for access to their simulations. We acknowledge support from HST-GO10937, HST-GO11563, HST-GO11144, and a Fulbright-CONICYT scholarship (V.G.). I.L. is supported by NASA through a Hubble Fellowship grant 51232.01-A awarded by the Space Telescope Science Institute.

REFERENCES

Bouwens, R. J., Illingworth, G. D., Franx, M., & Ford, H. 2007, ApJ, 670, 928
Bouwens, R. J., et al. 2010, ApJ, submitted (arXiv:1006.4360)
Bower, R. G., Benson, A. J., Malbon, R., Helly, J. C., Frenk, C. S., Baugh, C. M., Cole, S., & Lacey, C. G. 2006, MNRAS, 370, 645
Bruzual, G., & Charlot, S. 2003, MNRAS, 344, 1000
Choi, J., & Nagamine, K. 2010, MNRAS, 407, 1464
de Santis, C., Grazian, A., Fontana, A., & Santini, P. 2007, New Astron., 12, 271
Eyles, L. P., Bunker, A. J., Ellis, R. S., Lacy, M., Stanway, E. R., Stark, D. P., & Chiu, K. 2007, MNRAS, 374, 910
Eyles, L. P., Bunker, A. J., Stanway, E. R., Lacy, M., Ellis, R. S., & Doherty, M. 2005, MNRAS, 364, 443
Finlator, K., Davé, R., & Oppenheimer, B. D. 2007, MNRAS, 376, 1861
Finlator, K., Oppenheimer, B. D., & Davé, R. 2011, MNRAS, 410, 1703
Giavalisco, M., et al. 2004, ApJ, 600, L93
González, V., Labbé, I., Bouwens, R. J., Illingworth, G., Franx, M., Kriek, M., & Brammer, G. B. 2010, ApJ, 713, 115
Jaacks, J., Choi, J., & Nagamine, K. 2011, arXiv:1104.2345
Kriek, M., van Dokkum, P. G., Labbé, I., Franx, M., Illingworth, G. D., Marchesini, D., & Quadri, R. F. 2009, ApJ, 700, 221
Labbé, I., Bouwens, R., Illingworth, G. D., & Franx, M. 2006, ApJ, 649, L67
Labbé, I., et al. 2010a, ApJ, 716, L103
Labbé, I., et al. 2010b, ApJ, 708, L26
Madau, P., Pozzetti, L., & Dickinson, M. 1998, ApJ, 498, 106
Marchesini, D., van Dokkum, P. G., Förster Schreiber, N. M., Franx, M., Labbé, I., & Wuyts, S. 2009, ApJ, 701, 1765
McLure, R. J., Cirasuolo, M., Dunlop, J. S., Foucaud, S., & Almaini, O. 2009, MNRAS, 395, 2196
Oke, J. B., & Gunn, J. E. 1983, ApJ, 266, 713
Papovich, C., Dickinson, M., & Ferguson, H. C. 2001, ApJ, 559, 620
Papovich, C., Finkelstein, S. L., Ferguson, H. C., Lotz, J. M., & Giavalisco, M. 2011, MNRAS, 412, 1123
Salpeter, E. E. 1955, ApJ, 121, 161
Stark, D. P., Ellis, R. S., Bunker, A., Bundy, K., Targett, T., Benson, A., & Lacy, M. 2009, ApJ, 697, 1493
Windhorst, R. A., et al. 2011, ApJS, 193, 27
Wuyts, S., et al. 2007, ApJ, 655, 51
Yan, H., Dickinson, M., Giavalisco, M., Stern, D., Eisenhardt, P. R. M., & Ferguson, H. C. 2006, ApJ, 651, 24
Yan, H., et al. 2005, ApJ, 634, 109